Journal of Power Sources 182 (2008) 39–47

Contents lists available at ScienceDirect

Journal of Power Sources

journal homepage: www.elsevier.com/locate/jpowsour

Membrane degradation mechanism during open-circuit voltage hold test

Atsushi Ohma*, Shinji Yamamoto, Kazuhiko Shinohara

Nissan Research Center, Nissan Motor Co., Ltd., 1 Natsushima-cho, Yokosuka-shi, Kanagawa 237-8523, Japan

ARTICLE INFO

Article history:
Received 20 February 2008
Received in revised form 24 March 2008
Accepted 25 March 2008
Available online 7 April 2008

Keywords:
PEMFC
MEA
Durability
Hydrogen peroxide
Pt band
Pt-ion diffusion

ABSTRACT

A detailed analysis is made of the relation between the degradation behavior of a membrane electrode assembly (MEA) and deposited Pt (Pt band) in the membrane during an open-circuit voltage (OCV) hold test. Molecular-structural changes in the membrane are investigated by micro-Raman spectroscopy. When the Pt band was not significantly observed in the membrane after the test, the membrane is relatively stable. In contrast, when the Pt band was clearly formed, the membrane around it was intensively degraded. The magnitude of the fluoride ion emission rate (FER) of the effluent water from the anode and the cathode was also consistent with the location of the Pt band. It was verified that the Pt band is one of the factors accelerating membrane degradation, and the catalyst materials strongly affects the degradation. Besides, not the cation transport which enhances the degradation but the kinetics of either the H_2O_2 and/or hydroxyl radical production might be the rate determining step.

1. Introduction

Polymer electrolyte fuel cells (PEFCs) are a very promising power source for automotive use. There are challenges still remaining such as efficiency, durability, sub-zero startup, and cost reduction, etc. Some of recent research efforts have been focused on improving the durability of the membrane electrode assembly (MEA) during start–stop operation, load cycling and idling. In start–stop operation, an MEA is degraded due to cathode carbon corrosion which occurs when hydrogen is absent at the cathode while the remaining air at the anode is replaced by hydrogen [1–3]. In load cycling operation, cathode Pt dissolves to Pt ions due to potential cycling and the ions diffuse into the membrane, resulting in cathode electrochemical surface area (ECA) loss [4,5].

On the other hand, MEA degradation has not been thoroughly investigated under idling operation. Because the applied current density of an MEA is small during idling, the cathode potential of the MEA is high. Thus, it is thought that an open-circuit voltage (OCV) hold test can simulate idling operation. Quite a few membrane degradation phenomena during OCV hold tests have been reported so far [6–8]. The typical membrane degradation mechanism in an OCV state stems from hydrogen peroxide (H_2O_2) produced during the 2-electron oxygen reduction reaction (ORR) process at the anode [6]. The 2-electron ORR process can be expressed by the following pathway:

$$O_2 + 2H^+ + 2e^- = H_2O_2 \quad (E_0 = 0.672\,V) \tag{1}$$

So far the reaction above has been considered to occur mainly at the anode during the OCV hold duration due to its lower potential. However, another mechanism has been suggested recently that the reaction might occur at the deposited Pt (Pt band) in the membrane [9–13].

We also have been conducting a lot of OCV hold tests in various test conditions to date, and post-test analyses. Fig. 1 shows the typical cross-sectional SEM images of MEAs in the vicinity of the catalyst layer edge after the OCV hold tests. Two MEAs are shown, whose alignment of the anode and cathode catalyst layers were intentionally controlled contrary. In Case 1 where the anode was beyond the cathode, significant membrane thinning was not observed where the anode was beyond the cathode. In contrast, the membrane in the vicinity of where the cathode was beyond the anode was degraded to be thinned remarkably in Case 2, and the Pt band was also observed there. These results imply that the Pt band could accelerate the membrane thinning.

In our previous study [11,12], OCV hold tests were conducted using different gas compositions at both electrodes, and it was concluded that the location of the Pt band might correlate with the magnitude of the fluoride ion emission rate (FER) of the effluent water, and it was considered that the Pt band might enhance the membrane degradation. The hypothesis of why the Pt band accelerates the membrane degradation is considered as follows. Firstly, at the Pt band, the potential is considered around 0 V (vs. RHE) which is determined by the partial pressures of the hydrogen in

* Corresponding author. Tel.: +81 46 867 5174; fax: +81 46 867 5332.
E-mail address: a-ohma@mail.nissan.co.jp (A. Ohma).

0378-7753/$ – see front matter © 2008 Elsevier B.V. All rights reserved.
doi:10.1016/j.jpowsour.2008.03.078

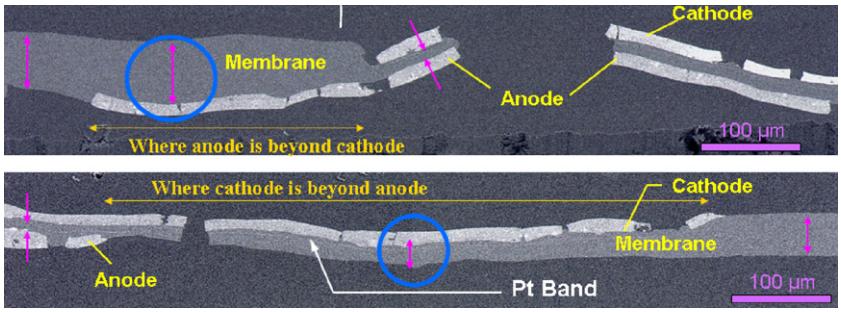

Fig. 1. Typical cross-sectional SEM images of MEAs in the vicinity of the catalyst layer edge (Case 1: anode is beyond cathode. Case 2: cathode is beyond anode.).

the anode and the oxygen in the cathode and their permeabilities of the membrane. Secondly, the distance to the Pt band from the cathode is closer than to the anode, which enhances the oxygen flux from the cathode. Thirdly, apparent density of the Pt particles in the Pt band, equivalent to the volume and/or mass fraction in the membrane, is normally lower than the anode and the cathode, resulting in lower ORR activity at the Pt band and higher 2-electron reaction rate. As a result, H_2O_2 formation rate probably becomes significantly higher, which accelerates the membrane degradation.

In this study, we investigated in more detail the relation between the Pt band and the membrane degradation behavior during the OCV hold duration in order to validate that the Pt band in the membrane is one of the factors accelerating membrane degradation in the hold interval. We also updated the membrane degradation mechanism.

2. Experimental

Perfluorosulfonic acid (PFSA) membranes (Nafion® NRE212-CS, thickness = 50 μm) were used in this study. It is chemically stabilized, in short, almost all the ends of the main chains are capped by fluorine. Catalyst ink was prepared by mixing Pt/C and the Nafion® ionomer solution (DE2020, EW1000, DuPont) together so that the weight ratio of the ionomer content was 0.9 relative to the carbon support. Two different catalyst materials (Catalysts A: 46 wt%, TEC10E50E, TKK, and B: 50 wt%, advanced) prepared in different processes were used. A propylene glycol solution (50 wt%) was also added to the catalyst ink to keep the solid content of the ink at 19 wt%. Electrocatalyst layers were fabricated on polytetrafluoroethylene (PTFE) substrates using a screen-printing technique. The square electrocatalyst layers measured 50 mm on one side and had a Pt loading of 0.35 mg cm^{-2}. The electrocatalyst layers were heat-treated on the PTFE substrates for 30 min at 130 °C to remove any organic solvent, and then decal transferred to the square membrane (72 mm on one side) to fabricate the catalyst-coated membranes (CCM, active area of 25 cm^2). The decal transfer conditions were 150 °C, 10 min, and 0.8 MPa. Polyethylene naphthalate (PEN) films (Q51, 25 μm, Teijin-DuPont) were bonded on the surrounding areas of the electrocatalysts as reinforcements. Carbon paper gas diffusion layers (GDLs) with a microporous layer (20BC, SGL Carbon) were used in this study. The MEAs were formed by assembling the GDLs on both sides of the CCM. An MEA was assembled in a single cell between bipolar plates (BPPs) made of graphite and gaskets made of silicone rubber. The compression pressure was kept uniform by measuring it with pressure-sensitive paper (Prescale, Fuji Film). Two samples with the different catalyst materials were prepared as explained here to conduct OCV hold tests under the same operating conditions. The catalysts of the anode and the cathode were the same in each sample.

Table 1 shows the OCV hold test conditions. In order to simplify the degradation phenomena and the analysis, the symmetric test conditions were adopted here between the anode and the cathode (i.e. pure H_2 and O_2, and 30% relative humidity for the both). As mentioned above, the only difference between samples 1 and 2 was their catalyst materials. After the OCV hold test, the deposited Pt in the membranes was observed using a transmission electron microscope (TEM). And an electron diffraction pattern of the selected Pt was obtained with 2° angle of incidence. The membrane degradation in the through-plane direction was investigated by means of micro-Raman spectroscopy, which is a powerful tool for analyzing molecular-structural changes in the membrane [14–16]. The fluoride and the sulfate ion concentrations from the anode and cathode effluent water during the tests were measured by ion chromatography (IC) in order to calculate the FER and the sulfate ion emission rate (SER).

Table 1
OCV hold test conditions

	Sample 1	Sample 2
Catalyst (anode and cathode)	Catalyst A (TEC10E50E, 46 wt%, TKK)	Catalyst B (advanced, 50 wt%, TKK)
Anode gas	H_2	H_2
Cathode gas	O_2	O_2
Cell temperature (K)	363	363
Back pressure	Ambient	Ambient
Anode dew point (K)	334	334
Cathode dew point (K)	334	334
Anode flow rate ($Nm^3\ min^{-1}$)	0.5×10^{-3}	0.5×10^{-3}
Cathode flow rate ($Nm^3\ min^{-1}$)	0.5×10^{-3}	0.5×10^{-3}
Duration of OCV hold (h)	48	48

3. Results and discussion

Fig. 2 shows typical OCV hold test results. The OCV of sample 1 remained steady without a significant voltage drop during the test. The OCV of sample 2 dropped noticeably within the first 10 h, and

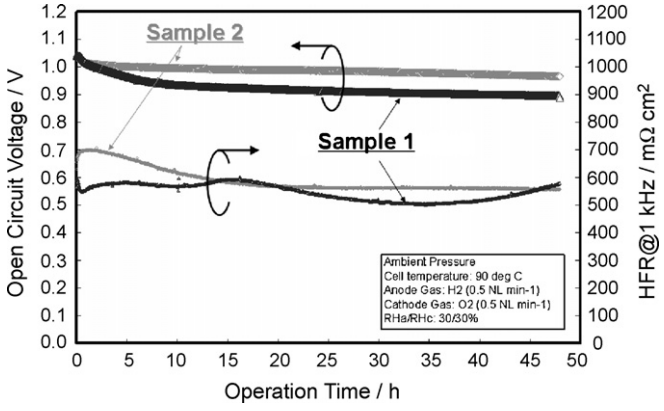

Fig. 2. OCV hold test results.

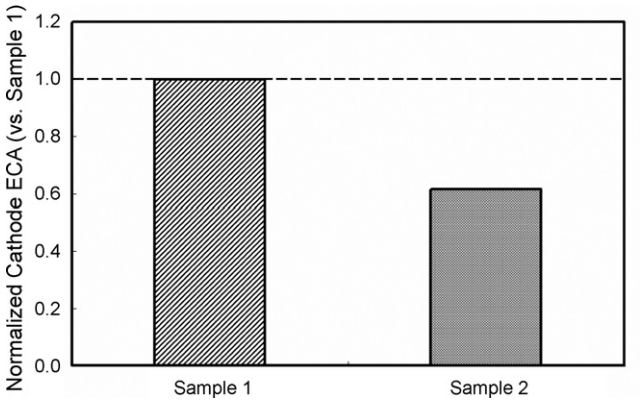

Fig. 3. Normalized cathode ECA.

then remained steady during the rest of the test. The OCV of sample 2 was higher than that of sample 1 during the tests. The change in the high frequency resistance (HFR) at 1 kHz was also steady in each sample.

Fig. 3 shows the normalized electrochemical surface area of the cathodes of samples 1 and 2 before the OCV tests. The value of sample 2 is shown in relation to a value of 1.0 for sample 1. The cathode ECA of sample 2 was around 60% of that of sample 1. According to a simple estimation, the kinetic loss of sample 2 was 15 mV greater than that of sample 1. However, as shown in Fig. 2, the OCV of sample 2 remained significantly higher than that of sample 1, indicating that the crossover current and/or the electronic shorting across the membrane may have increased during the test.

After the OCV hold tests, cross-sections of the central region of the tested MEAs were observed with a TEM. Fig. 4 shows TEM images of the two samples. Pt deposition in the membrane was confirmed in each sample. In sample 1, where Catalyst A was used on both the anode and the cathode, the Pt band, consisting of a lot of Pt particles, was clearly observed around the central region in the cross-sectional direction of the membrane. It is considered that the Pt band might be finally formed after the repetitive dissolution and reduction processes in the vicinity of the membrane close to the cathode [11,12]. The reduction process is chemical reaction shown in Eq. (2).

$$Pt^{2+} + H_2 = Pt + 2H^+ \quad (2)$$

Compared with the results of our previous studies, the location of the Pt band in sample 1 was a little bit closer to the cathode. As mentioned in Refs. [11,12], the location is basically determined by the partial pressures of H_2 and O_2 at both electrodes, and their permeabilities in the membrane. The partial pressure of H_2 is related to the back pressure, and that of O_2 is a function of the relative humidity [17]. Therefore, this slight difference in location could be due to

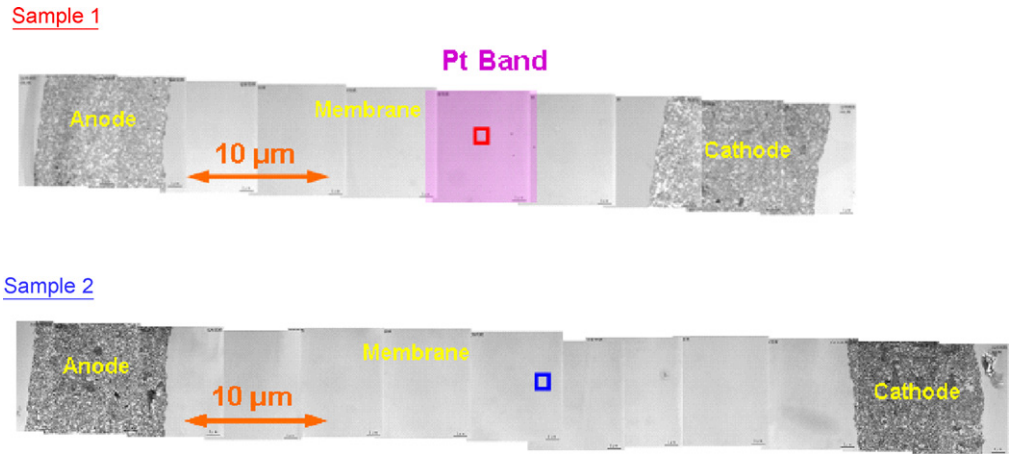

Fig. 4. TEM images of sample cross-sections.

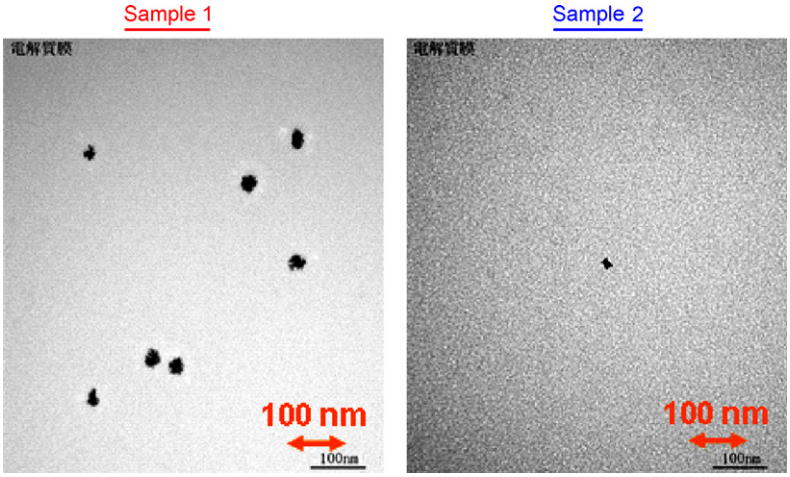

Fig. 5. Magnified TEM images of the Pt in the square areas of the membrane in Fig. 4.

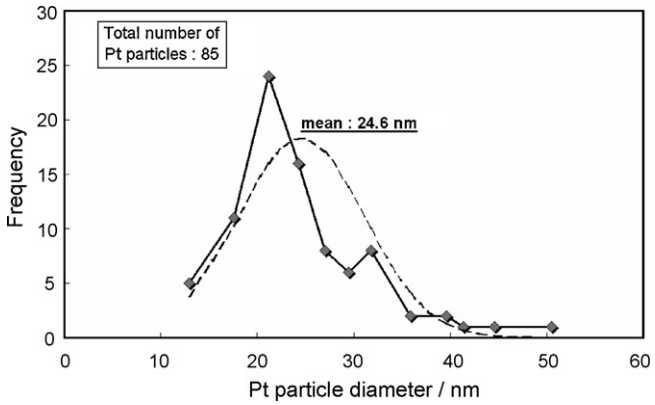

Fig. 6. Pt particle frequency as a function of the particle diameter in the Pt band of sample 1.

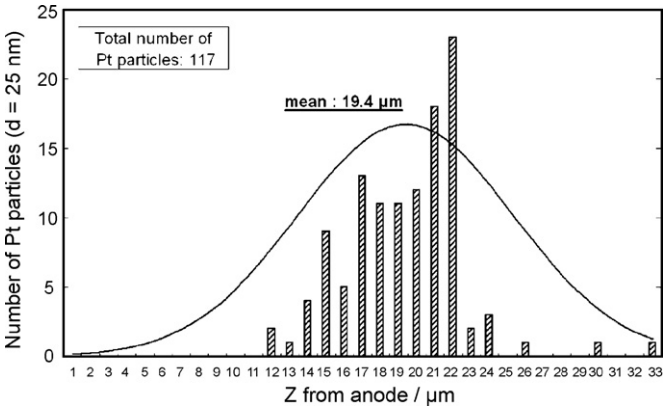

Fig. 8. Histogram of Pt particles through the cross-section of sample 1.

small differences in back pressures and/or dew points of the reactants. The membrane also became thinner than its initial thickness (50 μm).

In contrast, the Pt band was not clearly observed in sample 2, which had Catalyst B on both the anode and the cathode. Only a few Pt particles were observed in the membrane shown in Fig. 5. The membrane thickness also seemed to be stable.

Fig. 5 shows magnified TEM images of the Pt in the square areas of the membrane in Fig. 4. A lot of Pt particles, with an average diameter of about 25 nm, were observed in sample 1, whereas there were only a few Pt particles of about 15 nm in diameter in the membrane of sample 2. The apparent Pt density of sample 2 was notably lower than that of sample 1, which cannot be explained only by the difference in the cathode ECAs shown in Fig. 3.

Fig. 6 shows Pt particle frequency as a function of the particle diameter in the Pt band of sample 1. It was found that the diameter of around 80% of the particles was between 18 and 30 nm, and the mean value showed 24.6 nm. Pt particles might grow through the OCV duration and the diameter seemed saturated around 25 nm in this case, which may be relative to Gibbs–Thomas equation.

Furthermore magnified TEM image of the selected Pt particle and the electron diffraction pattern in sample 1 are shown in Fig. 7. A lot of Pt crystal grains form the Pt agglomerate whose diameter is about 25 nm. The diffraction pattern corresponds to the $[1\,\bar{1}\,\bar{2}]$ zone axis of the platinum crystal structure, indicating that the Pt particle is well-oriented. As mentioned above, though the Pt might be formed through the repetitive processes, it was also like a single crystal as well as the deposited Pt in the ionomer phase at the cathode in reference [18], where nitrogen was supplied to the cathode and hence the Pt ion was chemically deposited to be the Pt metal through non-repetitive reduction process.

The number of the deposited Pt particles was investigated in more detail from the TEM image of sample 1. Fig. 8 shows histogram of Pt particle distribution across the membrane in sample 1. The total number of Pt particles, whose diameter was almost about 25 nm except a few particles, was 117, and they were estimated to exist in the rectangular cross-section of approximate 0.5 μm^2 (5 μm wide × 0.1 μm thickness), so the apparent geometric-density of the Pt particles can be roughly calculated. According to the histogram, the width of the Pt band was around 10 μm, and the mean distance of the Pt particles was 19.4 μm from the anode.

The distribution of the Pt particles is quite characteristic. There are not many Pt particles between 33 and 23 μm from the anode, and the number of the particles remarkably increases around 22 μm, and then gradually decreases with decrease of the distance from the anode. This also indicates that the deposited Pt particles are probably formed through the repetitive dissolution and reduction processes as mentioned above.

To analyze how to form the Pt band in sample 1, simple model of the Pt ion transport through the membrane was considered here. The steady-state Pt ion transport model by Fick's law with the chemical reduction reaction of the Pt ion shown in Eq. (2) was considered as follows:

$$D^{\mathrm{eff}}_{\mathrm{Pt}^{2+}} \frac{\mathrm{d}^2 c_{\mathrm{Pt}^{2+}}}{\mathrm{d}x^2} - k c_{\mathrm{Pt}^{2+}} \frac{x}{L} = 0 \tag{3}$$

$$n = \frac{N_{\mathrm{Pt}^{2+}} t m_{\mathrm{a}}}{\rho(\pi \bar{d}^3/6)} \tag{4}$$

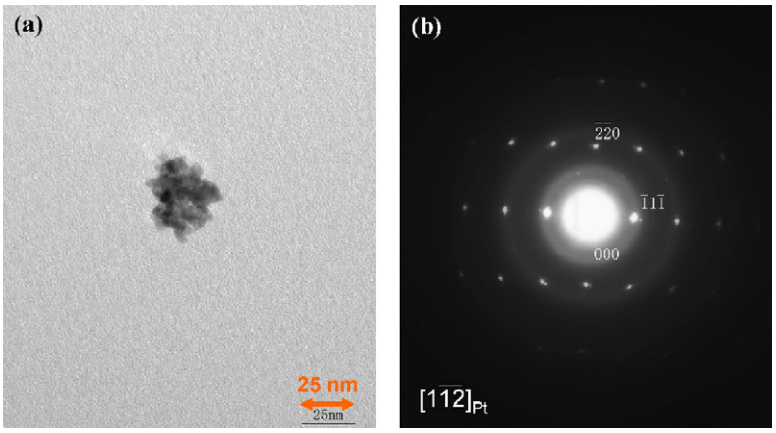

Fig. 7. (a) Magnified TEM image of a Pt particle in sample 1 and (b) the zone axis diffraction pattern.

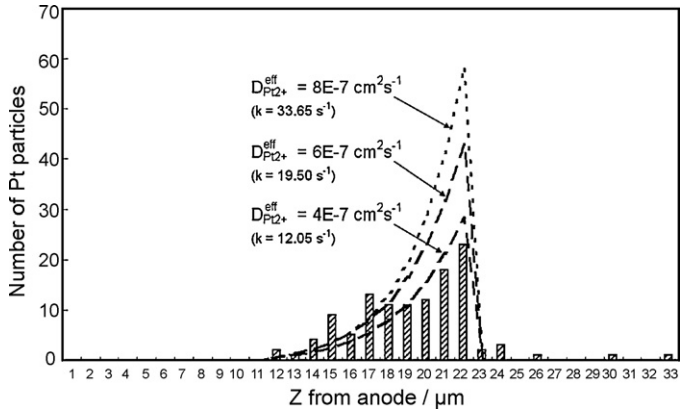

Fig. 9. Estimated Pt particle distribution at the EOL for different diffusion coefficients of Pt ions and reaction rate constants.

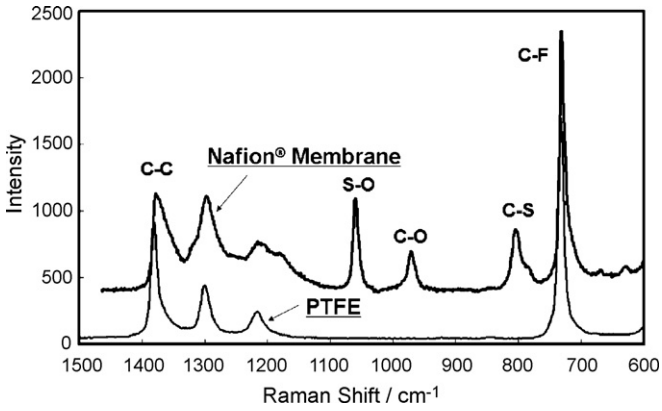

Fig. 10. Typical micro-Raman spectra.

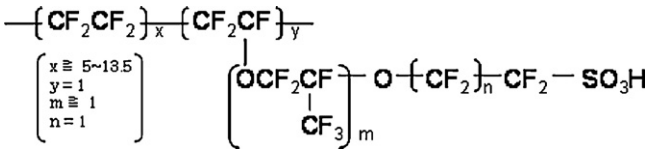

Fig. 11. Molecular structure of Nafion®.

where $D^{eff}_{Pt^{2+}}$ is effective diffusion coefficient of Pt ion in the membrane, $c_{Pt^{2+}}$ is local concentration of Pt ion at the cathode, k is the reaction rate constant of the chemical reduction which is explained later, x is the distance from the cathode, L is the membrane thickness at the end of the OCV duration (EOL) obtained by the TEM image (33 μm), $N_{Pt^{2+}}$ is Pt ion flux ($= -D^{eff}_{Pt^{2+}}(dc_{Pt^{2+}}/dx)$), n is estimated number of the Pt particles (counts cm^{-2}), t is the duration of the OCV hold test (48 h), m_a is atomic mass of Pt (195.1), ρ is density of Pt (21.45 g cm^{-3}), and $\bar{d}$ is the average Pt particle diameter (25 nm). According to Eq. (2), the chemical reduction reaction rate k' is considered in the following equation:

$$k' = k''[Pt^{2+}][H_2] = kc_{Pt^{2+}}\frac{x}{L} \quad (k = 0 \ \text{ when } 0 \leqq x \leqq 10) \tag{5}$$

Here k' is proportional to the Pt ion concentration, and hydrogen partial pressure which is a linear function of the relative distance from the cathode (x/L). Thus k is regarded as the rate constant. When x is 0–10 μm, k is considered as zero because the deposited Pt suddenly dissolves again resulting that the chemical deposition does not occur apparently.

During the OCV hold test of sample 1 shown in Fig. 2, the average cathode potential was about 0.9 V. Then $c_{Pt^{2+}}$ at $x = 0$ μm is estimated to be 1.0×10^{-7} M, and $D^{eff}_{Pt^{2+}}$ is around 8×10^{-7} cm^2 s^{-1} according to Ref. [18] where the same catalyst was used as Catalyst A (TEC10E50E, TKK) in this study. However, the effective diffusion coefficient in the OCV hold test might be actually lower than the above value, because the relative humidity of the reactants of the test was 30%, where water diffusion was not so fast as fully humidified condition. From the histogram of the Pt particle distribution obtained by the TEM result, the boundary conditions were determined that the Pt ion flux is negligibly small at $x = 22$ μm and the $c_{Pt^{2+}}$ at $x = 0$ μm is 1.0×10^{-7} M. Therefore $D^{eff}_{Pt^{2+}}$ and k are the fitting parameters here.

Fig. 9 shows estimated Pt particle distribution at the EOL with the different $D^{eff}_{Pt^{2+}}$ and k. It is well fitted when $D^{eff}_{Pt^{2+}}$ is 4×10^{-7} cm^2 s^{-1} which is half of the above value, suggesting it is reasonable considering the low RH. Note that this calculation was done under the simple assumption, where change in the membrane thickness and Pt ion solubility during the OCV duration were not accounted here, and average Pt particle diameter was assumed 25 nm relative to the mean value in Fig. 6.

In addition to the TEM analysis, micro-Raman spectroscopy was also used in this study to investigate the degradation profile of the molecular structure across the membrane after the OCV tests and to examine the relation to the Pt band.

Fig. 10 shows typical micro-Raman spectra of the Nafion® membrane and polytetrafluoroethylene, which is similar in basic molecular structure to Nafion®. Compared with the spectra of PTFE, pronounced peaks originating from the stretching vibration of single bonds of S–O, C–O, and S–C are observed around 1070, 970, and 810 cm^{-1}, respectively [19]. The single bonds are derived from the molecular structure of a side chain of Nafion® as shown in Fig. 11. The relative changes in these single bonds might be detected by comparing their intensities with that of C–F, which was present in a large amount in the membrane. The peak of the C–C single bond is seen around 1380 cm^{-1}. Because FWHM of the C–C bond of PTFE was much smaller than that of Nafion®, it is assumed that the FWHM became narrower relative to the degradation of the side chains.

Fig. 12 shows micro-Raman spectra of the membrane of sample 1 obtained at specific locations across the membrane. The spectra at positions 1, 3, 6, 24 and 27 μm from the anode were almost stable. The spectra at 12, 18, and 21 μm were different from the others, especially that at 18 μm.

From the spectra, the relative intensities of S–O and C–O vs. C–F, and the FWHM of C–C were calculated as a function of the fractional

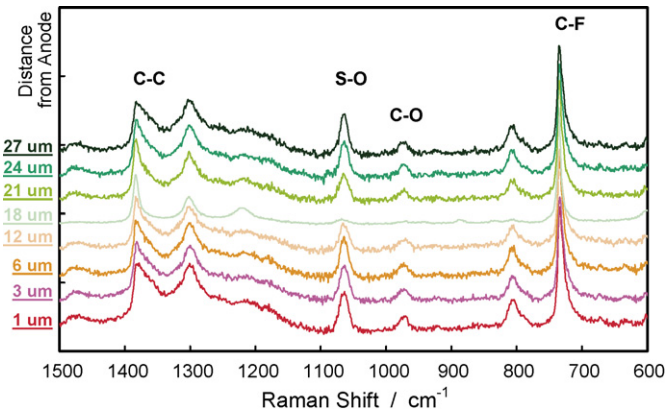

Fig. 12. Micro-Raman spectra at specific locations across the membrane of sample 1.

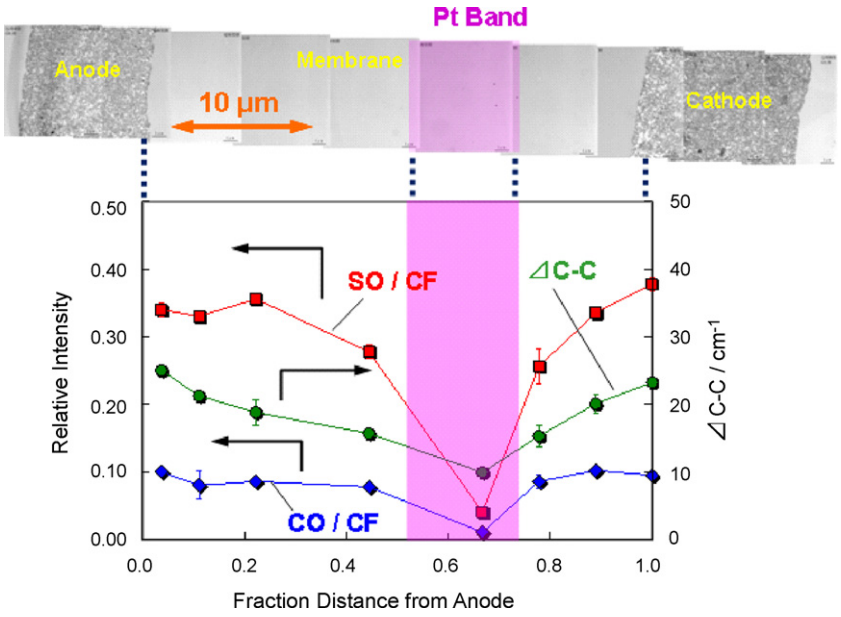

Fig. 13. Relative intensities of S–O and C–O vs. C–F and FWHM of C–C as a function of the fractional distance from the anode (sample 1).

distance from the anode. Fig. 13 shows the relation between them and the location of the Pt band in the membrane. Because the cross-section of the TEM image was very close to, but not completely the same as, that used in micro-Raman spectroscopy, the membrane thickness differed slightly within about 20%. Thus, the fractional distance was used here. The relative intensities and the FWHM at the Pt band were markedly lower than at the other locations across the membrane in sample 1, indicating that the side chains were especially decomposed around the Pt band.

As easily understood from Figs. 8 and 13, from more microscopic point of view, the profiles of the relative intensities were well consistent with the Pt particle distribution across the membrane, implying that the membrane decomposition might be remarkably relevant to the deposited Pt particles in the membrane. Besides, according to the rough estimation, the volume fraction of the Pt particles in the membrane is around ppm order, indicating the Pt particles could not affect the Raman-spectra.

In contrast, as shown in Fig. 14, they were relatively stable across the membrane in sample 2, where the Pt band was not clearly observed.

According to the results of the micro-Raman spectroscopy, it is obvious that the specification of the catalyst is important as well as that of the membrane to mitigate the membrane degradation.

One factor of the catalyst is how much Pt is dissolved into the ionomer. As shown in Figs. 4 and 5, the apparent density of the deposited Pt particles in sample 2 was significantly lower than that of sample 1, which could not be interpreted only by the difference of the cathode ECA in Fig. 3. It is not sure why Catalyst B is more durable than Catalyst A against the dissolution outside the field of the difference of the ECA. Though the Pt band strongly affects the membrane degradation, the significant difference of the membrane

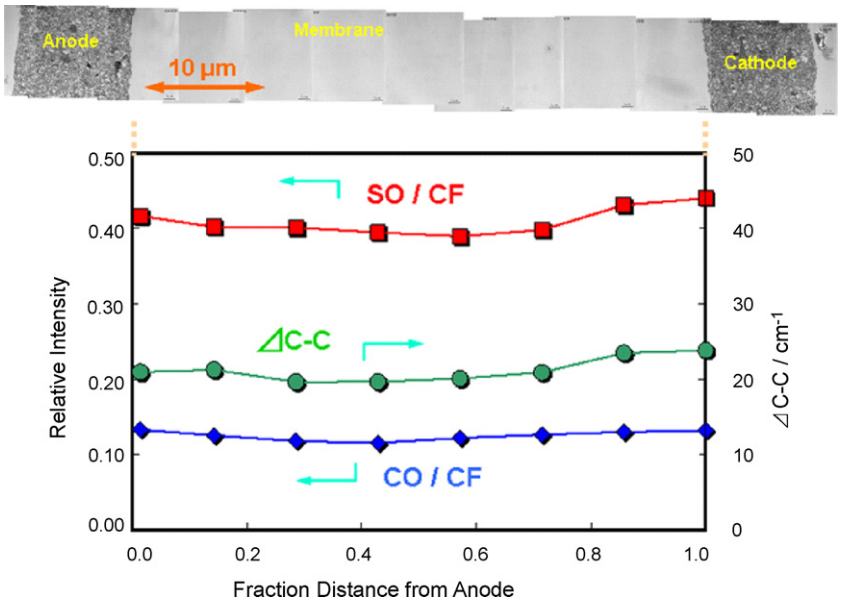

Fig. 14. Relative intensities of S–O and C–O vs. C–F and FWHM of C–C as a function of the fractional distance from the anode (sample 2).

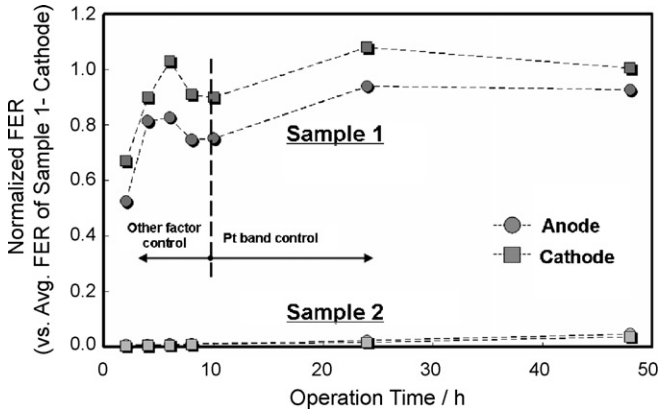

Fig. 15. Change in FERs during OCV hold test.

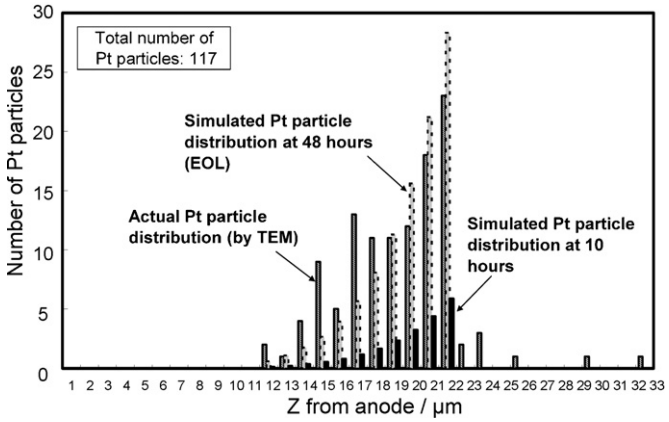

Fig. 16. Estimated Pt particle distribution in the membrane.

degradation behavior between the two samples, however, was not only due to whether there was a clear Pt band or not.

Another factor could be impurities in the catalyst. It is expected that Catalyst A has much impurities than Catalyst B. It has been said that the impurities such as cations accelerate the membrane degradation so far [6]. In our previous studies [11,12], it was indicated that H_2O_2 might be produced at the Pt band. On top of that, it was found that the membrane was remarkably degraded around the Pt band in the membrane in this study. Considering these phenomena, how the Pt band accelerates the membrane degradation is speculated as follows. As mentioned above, H_2O_2 might be produced at the Pt band. Because the degraded region of the membrane was just around the Pt band, the impurities may be sufficiently transported to the H_2O_2. In short, the transport of the impurities may not be limiting. Therefore, other factors such as the kinetics of either the H_2O_2 and/or hydroxyl radical production could be limiting. Another possibility is so-called direct hydroxyl radical formation on the Pt surface [9,13].

Anyway, the catalyst materials do affect the membrane degradation very much. Thus, the catalyst design is important in terms of the mitigation strategy of the membrane degradation.

Fig. 15 shows the change in the normalized FERs of the two samples as calculated from the fluoride ion concentration measured by IC in the effluent water from the anode and the cathode. The FER, which is an indicator of membrane degradation behavior, was normalized relative to the average FER of sample 1 from the cathode, which will be mentioned later. The FER during a certain period of time was calculated from the product divided by time; the product was derived by multiplying the ion concentration by the weight of the effluent water. The FERs shown here were corrected by subtracting the background. The FERs of sample 1 increased sharply in the first 6 h and then decreased until around 10 h, after which they increased again gradually. These unique trends could be relevant to the process of Pt band formation during the test.

One of the possibilities is that there are multiple steps of the fluoride ion emission with different limiting factors. In this case, it seems that there are roughly two steps of the emission. The first step is the initial 10 h, and the second step is the remaining duration. According to the following estimation, the latter could be limited by the Pt band formation, and the former may be determined by another factor.

Fig. 16 shows estimated Pt particle distribution at 48 h (EOL) and 10 h using the fitted diffusion coefficient of Pt ion (4×10^{-7} cm^2 s^{-1}) shown in Fig. 9. Pt band might be formed at 10 h which consists of more than total 20 of the Pt particles, assuming that the average Pt particle diameter is 25 nm. It is speculated that the roughness factor of the cathode might be larger than that of 48 h during the first 10 h, enhancing relatively the Pt dissolution in the first 10 h. In addition, the Pt particles in the membrane could be smaller than 25 nm because they were in the growing process at 10 h, indicating that there are so adequate Pt particles that the membrane degradation is possibly accelerated.

On the other hand, the FERs of sample 2 were significantly lower than those of sample 1. Probably the Pt band formation is not the dominant factor of the fluoride emission in sample 2.

Fig. 17 shows the normalized average FER relative to that of sample 1 from the cathode, which was calculated from the cumulative fluoride emission divided by the OCV duration. The FERs from the anode and the cathode were roughly even in samples 1 and 2. Obviously, the FERs of sample 2 were markedly lower than those of sample 1.

In addition, normalized cumulative fluoride emission of samples 1 and 2 relative to the total fluorine content in the MEA including both the membrane and the ionomer in the electrodes, and the fluorine from the main chains and the side chains is separately shown in the graph. The cumulative fluoride emission of sample 1 was about one-third of the total of the MEA. As mentioned before, the chemically stabilized Nafion® membrane (NRE212-CS) whose ends of the main chains were capped with fluorine was used in this study. In addition, according to the micro-Raman result, some of the exhausted fluoride of sample 1 was from the side chains. However, the cumulative fluoride emission was more than the total fluorine from the side chains, so both the side chains and the main chains were probably decomposed. Considering that the ends of the main chains were capped to be chemically stabilized, the main

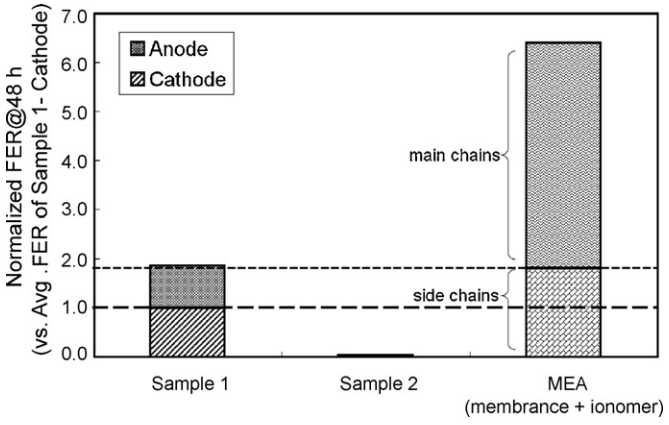

Fig. 17. Normalized average FER.

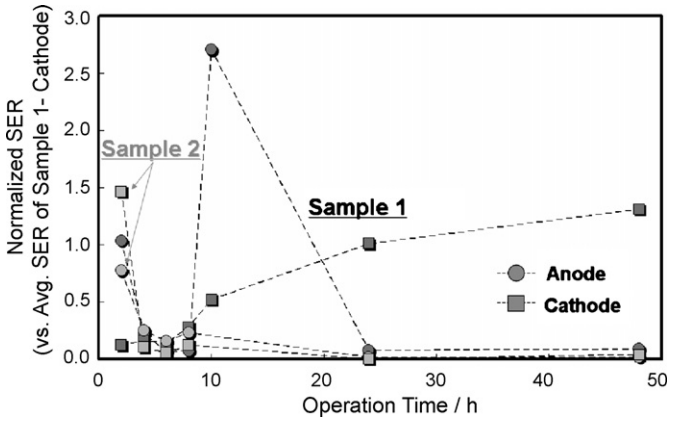

Fig. 18. Change in SERs during OCV hold test.

chain decomposition could begin at the branch point of the side chains, especially C–O bond to the side chain shown in Fig. 10.

Furthermore, the magnitude of the normalized FER was roughly consistent with the Pt band location in sample 1 because during approximately four-fifth of the OCV duration (10–48 h), the Pt band might control the membrane degradation, which suggests that fluoride ions were exhausted from either the anode or the cathode; the magnitude of the FERs was inversely proportional to the fractional distance from the electrodes. Because the Pt band was located a little bit closer to the cathode in this study, the cathode FER was probably slightly greater than that of the anode. However, the results for sample 2 show a discrepancy in this theory, indicating that some other factors might govern the membrane degradation.

Fig. 18 shows the change in the normalized SERs of the two samples as calculated from the sulfate ion concentration measured by IC in the effluent water from both electrodes. The SER, an indicator of decomposition of the side chains of the membrane, was normalized relative to the average SER of sample 1 from the cathode, as was done for the FER. The SERs were also corrected by subtracting the background. The cathode SER of sample 1 increased gradually after 8 h, and the anode SER seemed unstable compared with that of the cathode. The SERs of sample 2 were stable after 8 h. However, it has been reported that some of the sulfate ions might remain in the MEA [20]. Therefore, it is difficult to estimate when the decomposition of the side chains started accurately. Besides, judging from the higher SERs at the beginning, the some of the side chains could be decomposed even during the initial conditioning.

The normalized average SER relative to that of sample 1 from the cathode is shown in Fig. 19. For sample 1, the cathode SER was notably greater than that of the anode. The same tendency was confirmed for sample 2. The total SERs of sample 2 were much lower than those of sample 1, which was qualitatively consistent with the FER results. It is assumed that more ions would be present at the electrodes, so further study is necessary to analyze the behavior of the SER. Anyway, it is clear that the side chains of the membrane were decomposed because the sulfate ion was detected in the effluent water.

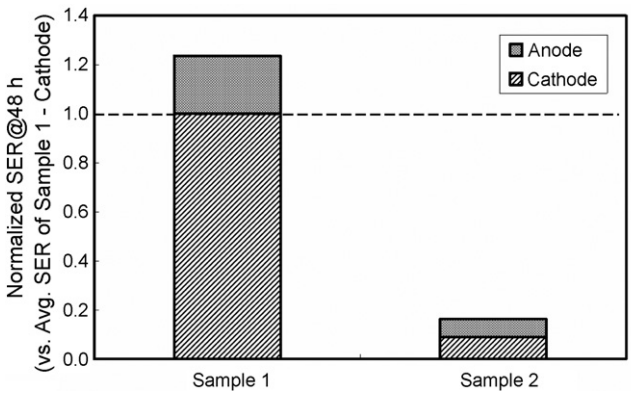

Fig. 19. Normalized average SER.

4. Conclusions

As one study in a series for improving the durability of MEAs for automotive use, the correlation between membrane degradation behavior and deposited Pt (Pt band) in the membrane during OCV hold tests was investigated in more detail in order to validate that Pt band formation is one of the factors accelerating degradation. Two MEA samples with different catalyst materials were tested.

After the OCV hold tests, cross-sections of the samples were observed with a TEM to investigate the Pt band. It was found that the Pt band consisting of a lot of Pt particles was clearly formed in sample 1, whereas it was not observed in sample 2. The effective diffusion coefficient of Pt ion was calculated from the simple steady-state diffusion model by fitting the estimated Pt particle distribution to the actual profile obtained by the TEM image.

Membrane degradation in the through-plane direction was then investigated by micro-Raman spectroscopy to analyze molecular-structural changes in the membrane. It was confirmed that the membrane around the Pt band in sample 1 was markedly degraded compared with the rest of the membrane. The degradation might be due to the decomposition of the side chains. In contrast, the membrane was not locally decomposed in sample 2, where the Pt band was not clearly seen. The micro-Raman results also imply that the kinetics of either the H_2O_2 and/or hydroxyl radical production, not the cation transport which enhances the degradation, might be the rate determining step.

During the OCV tests, the fluoride ion concentration in the effluent water, which is one of the indicators of membrane degradation, was measured by IC to calculate the FERs. The magnitude of the FERs was consistent with the location of the Pt band in the membrane in sample 1, which agreed with the results of micro-Raman spectroscopy. The cumulative fluoride ion emission was more than total fluorine content of the side chains in the MEA, indicating both the side chains and the main chains might be decomposed. The concentration of the sulfate ions, probably relevant to the decomposition of the side chains, was also measured to evaluate the SERs. It was found that sulfate ions were significantly measured from both electrodes, but this finding has not been quantitatively validated yet.

Based on the results of this study, we conclude that the Pt band formed in the membrane during the OCV hold duration is one of the factors which accelerates membrane degradation in the hold interval, and the catalyst materials strongly affects the degradation. In addition, not the cation transport which enhances the degradation but the kinetics of either the H_2O_2 and/or hydroxyl radical production might be the limiting factor.

Acknowledgements

We gratefully acknowledge the Toray Research Center for their analysis of the micro-Raman spectra and valuable discussions.

References

[1] C.A. Reiser, L. Bregoli, T.W. Patterson, J.S. Yi, J. Deliang Yang, M.L. Perry, T.D. Jarvi, Electrochem. Solid-State Lett. 8 (2005) 273.

[2] J.P. Meyers, R.M. Darling, J. Electrochem. Soc. 153 (2006) 1432.
[3] L.M. Roen, C.H. Paik, T.D. Jarvi, Electrochem. Solid-State Lett. 7 (2004) 19.
[4] X. Wang, R. Kumar, D.J. Myers, Electrochem. Solid-State Lett. 9 (2006) 225.
[5] R.M. Darling, J.P. Meyers, J. Electrochem. Soc. 150 (2003) A1523.
[6] A.B. LaConti, M. Hamdan, R.C. McDonald, Handbook of Fuel Cells—Fundamentals, Technology and Applications, vol. 3, John Wiley & Sons, New York, 2003 (Chapter 49).
[7] E. Endoh, S. Honmura, S. Terazono, H. Widjaja, Y. Takimoto, 205th Meeting of the Electrochemical Society, Hawaii, October, 2004.
[8] V.O. Mittal, H. Russell Kunz, J.M. Fenton, Electrochem. Solid-State Lett. 9 (2006) A299.
[9] S. Burlatsky, N. Cipollini, D. Condit, T. Madden, V. Atrazhev, 208th Meeting of the Electrochemical Society, Los Angeles, October, 2005, Abstract #1189.
[10] V. Mittal, H.R. Kunz, J.M. Fenton, 208th Meeting of the Electrochemical Society, Los Angeles, October, 2005, Abstract #1192.
[11] A. Ohma, S. Suga, S. Yamamoto, K. Shinohara, ECS Trans. 3 (1) (2006) 519–529.
[12] A. Ohma, S. Suga, S. Yamamoto, K. Shinohara, JES 154 (2007) B757.
[13] N.E. Cipollini, Mater. Res. Soc. Symp. Proc. 885E (2006).
[14] H. Ericson, T. Kallio, T. Lehtinen, B. Mattsson, G. Sundholm, F. Sundholm, P. Jacobsson, J. Electrochem. Soc. 149 (2) (2002) A206–A211.
[15] H. Matic, A. Lundblad, G. Lindbergh, P. Jacobsson, Electrochem. Solid-State Lett. 8 (1) (2005) A5–A7.
[16] Y. Aoki, G. Katagiri, H. Nakayama, M. Hori, Proceedings of the 47th Battery Symposium, Japan, Tokyo, November, 2006, Abstract 2P-36.
[17] S. Takaichi, H. Uchida, M. Watanabe, Electrochem. Commun. 9 (2007) 1975.
[18] P.J. Ferreira, G.J. la O', Y. Shao-Horn, D. Morgan, R. Makharia, S. Kocha, H.A. Gasteiger, JES 152 (11) (2005) A2256.
[19] H. Nakayama, T. Minamide, M. Hori, Y. Sakiyama, Y. Aoki, K. Okubo, G. Katagiri, Proceedings of the 14th FCDIC Fuel Cell Symposium, Tokyo, May, 2007, p. 103.
[20] M. Gemba, S. Kosako, Y. Tsuji, The 73rd Meeting of The Electrochemical Society of Japan, Tokyo, April, 2006, Abstract 3P-29.